ISIJ International, Vol. 52 (2012), No. 3, pp. 434–440

Effects of Second Phase Particle Dispersion on Kinetics of Isothermal Peritectic Transformation in Fe–C Alloy

Liang CHEN,[1)]* Kiyotaka MATSUURA,[2)] Daisuke SATO[1)] and Munekazu OHNO[2)]

1) Graduate Student, Graduate School of Engineering, Hokkaido University, Kita 13 Nishi 8, Kita-ku, Sapporo, Hokkaido, 060-8263 Japan. E-mail: chenliang@eng.hokudai.ac.jp, SATO_soshiki@frontier.hokudai.ac.jp 2) Division of Materials Science and Engineering, Faculty of Engineering, Hokkaido University, Kita 13 Nishi 8, Kita-Ku, Sapporo, Hokkaido, 060-8263 Japan. E-mail: matsuura@eng.hokudai.ac.jp, mohno@eng.hokudai.ac.jp

(*Received on July 28, 2011; accepted on October 25, 2011*)

Effects of dispersion of insolvable particles on peritectic transformation kinetics in Fe–C binary alloy system have been investigated by means of a model experiment based on a diffusion couple method. During isothermal holding of the diffusion couple of δ and liquid phase samples, the peritectic transformation proceeds by migrations of ferrite(δ)/austenite(γ) interface and liquid(L)/γ interface. It was observed that the existence of insolvable particle, ZrO_2, in δ phase retarded the migration of δ/γ interface and also the migration of L/γ interface. The retarding effect by the ZrO_2 particles becomes strong as volume fraction of particles increases and/or particle radius decreases, which is qualitatively coincident with the effect of particles on grain growth (Zener pinning). These findings were verified by multi-phase field simulations.

KEY WORDS: peritectic transformation; Fe–C system; second phase particles; retarding effect; diffusion couple; multi-phase field.

1. Introduction

It is known that during continuous casting processes of peritectic carbon steels coarse austenite (γ) grains are usually formed, which causes harmful effects on hot ductility and the occurrence of surface cracking of the cast slabs.[1)] Therefore, the formation of coarse γ grains is one of the major problems in the continuous casting processes. In peritectic carbon steels, ferrite (δ) or liquid phase inhibits γ grain growth during the peritectic transformation in $\delta+\gamma$ or L+γ two-phase field following the peritectic reaction L+$\delta\rightarrow\gamma$. Rapid grain growth of γ phase takes place at high temperatures immediately after the completion of the transformation into γ single phase at a temperature which is denoted as T_γ in this paper. Therefore, the decrease in T_γ corresponds to a decrease in the temperature for onset of rapid grain growth, thereby retarding γ grain growth at high temperatures. In fact, it has been reported in several studies[2–5)] that reduction of T_γ by alloying element addition leads to grain refinement of as-cast γ structure. It should be noted that these early works focused on the reduction of T_γ due to stabilization of liquid or δ phase in a low temperature region. To the best of authors' knowledge, there has not been any attempt made for the reduction of T_γ due to retardation of the peritectic transformation process by insoluble particles, which is our main concern in this study.

In the peritectic reaction, liquid and δ phases react to form γ phase which leads to a thin γ phase film separating the liquid and δ phases. The peritectic reaction proceeds by the migration of triple junction between liquid, δ and γ phases. Shibata *et al.*[6)] and Phelan *et al.*[7)] performed in-situ observations by means of confocal scanning laser microscope, demonstrating that this reaction proceeds at quite high velocities of several mm/s. The fact that the peritectic reaction occurs at very high rates has been confirmed by recent phase field simulations.[8)] After this fast reaction process, the liquid and δ phases are completely separated by γ phase. Then, δ to γ transformation and liquid to γ solidification, *i.e.*, the peritectic transformation takes place and the thickness of the γ phase film increases. The kinetics of peritectic transformation in Fe–C binary alloys has been investigated in both experimental and numerical works. Matsuura *et al.*[9–11)] performed model experiments using a solid/liquid diffusion couple and demonstrated that δ/γ interface migrates at much higher velocity than L/γ interface. This evidence has been verified by finite difference simulations for carbon diffusion[9–13)] and phase field simulations.[8)]

It should be pointed out that the findings mentioned above were obtained for planar interfaces moving without any obstacle. The pinning effect of insoluble particles on grain growth has been widely studied[14–17)] and the theoretical treatment was firstly proposed by Zener.[18)] When the grain growth is considered, the driving force is associated with the reduction of total amount of grain boundary energy. Hence, the retarding effect by the insoluble particle is fully determined in the light of the reduction of total amount of grain boundary energy. On the other hand, when the motion of δ/γ interface is considered, the driving force originates from the difference in the chemical potential between δ and γ phases. The kinetics of this interface motion is generally diffusion-controlled. Hence, the retarding effect of insoluble particles on peritectic transformation should not be deter-

mined by only the reduction of total amount of interface energies. However, if insolvable particles exist in δ phase and are contact with the moving δ/γ interface, the amount of δ/γ interfacial energy associated with the contact area should vanish. Then, the migration of δ/γ interface passing over the particles involves the increase of the amount of interfacial energy. Therefore, it is highly expected that the migration of δ/γ interface during the peritectic transformation should be retarded as is similar to the phenomenon known as pinning effect on grain growth.

The main purpose of the present study is to clarify whether or not the pinning effect of dispersed particles on migration of δ/γ interface during the peritectic transformation exists and also to investigate the effects in terms of different volume fractions and radii of the second phase particles. For this, we carry out the diffusion couple experiment by which the migration velocities of δ/γ and L/γ interfaces during the peritectic transformation can be measured. It will be demonstrated that the migration of δ/γ interface is retarded by the particles dispersed in δ phase. Interestingly, the existence of particles in δ phase also reduces the migration velocity of L/γ interface. As is similar to the Zener pinning, the retarding effect on δ/γ and L/γ interfaces becomes significant when volume fraction is high and/or the particle size is small. In the present study, furthermore, these findings are verified by means of multi-phase field simulations.

2. Experimental Procedures

We carried out the diffusion couple experiment which is essentially the same as that proposed in Ref. 9). **Figure 1** shows the equilibrium phase diagram of Fe–C binary alloy.[19] When δ solid sample with 0.04 mass% carbon and liquid sample with 1.25 mass% carbon are held in contact with each other at 1 718 K, γ phase appears in between these samples. The thickness of the γ phase increases with increasing holding time. Importantly, the γ phase grows toward δ solid sample by δ to γ transformation and toward liquid sample by liquid to γ solidification. Then, the migrations of δ/γ and L/γ interfaces can be investigated in detail. In the present study, the insolvable particles, more specifically, ZrO_2 spherical particles are dispersed in the δ solid sample and the migration of δ/γ and L/γ interfaces is investigated in the diffusion couple experiment. The procedures are explained below.

We focused on the holding temperature of 1 718 K. The liquid sample of Fe-1.25 mass% C alloy was prepared by mixing an Fe-4.5 mass% C alloy and pure iron. The δ solid sample containing uniformly dispersed ZrO_2 particles was prepared as follows. Pure iron powder of 150 μm in diameter was mixed with ZrO_2 particles by ball milling for 1 hour, and then the mixture was hot pressed at 1 373 K into a cylindrical shape having a diameter of 25 mm and a height of 25 mm. After contact with liquid sample at 1 718 K, this pure iron δ solid sample receives carbon from liquid sample and its carbon concentration increases up to the equilibrium value, viz., 0.04 mass% in a short time. The radius, r and volume fraction, f_v of the ZrO_2 particles were varied from r=15 to 50 μm and from f_v=0.02 to 0.3, respectively. The purities of liquid and δ solid samples without ZrO_2 were Si<0.01, Mn<0.01, P<0.002, S<0.002 and Al<0.001 mass%.

The liquid sample thus prepared was put in an Al_2O_3 crucible with an inner diameter of 34 mm and a depth of 135 mm and the crucible was held inside a SiC electric furnace at 1 843 K with flowing Ar atmosphere. As schematically illustrated in **Fig. 2**(a), the δ sample was suspended by a thin Al_2O_3 tube from the upper part of the furnace at which the temperature is about 1 000 K. After the liquid sample was completely melted, the furnace was cooled to 1 718 K with a cooling rate of 0.028 K/s. During this cooling process, the δ sample was slowly moved to the position just above the liquid sample inside the crucible. When both samples reached 1 718 K after holding for 10 min, the δ sample was slightly moved down to have a contact with the liquid sample, as shown in Fig. 2(b). When a predetermined time passed, the thin Al_2O_3 tube joined with the δ sample was broken rapidly and the diffusion couple was quickly dropped into strongly stirred iced water to quench the diffusion couple sample.

The quenched diffusion couple was sectioned longitudinally and the sectioned surface was etched with a 3 vol% Nital solution after polishing. The thickness of γ phase formed from the δ and liquid phases was measured using an optical microscope.

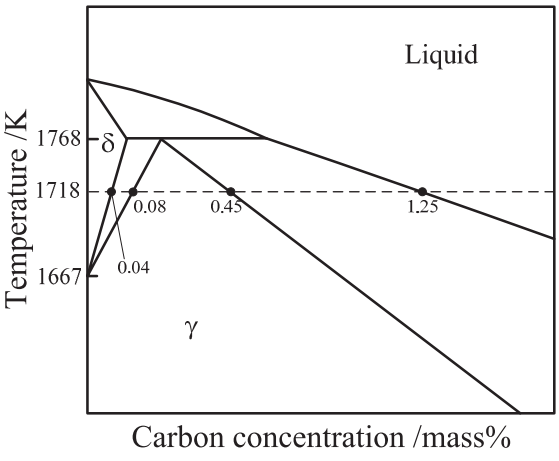

Fig. 1. Equilibrium phase diagram of Fe–C binary alloy.[19]

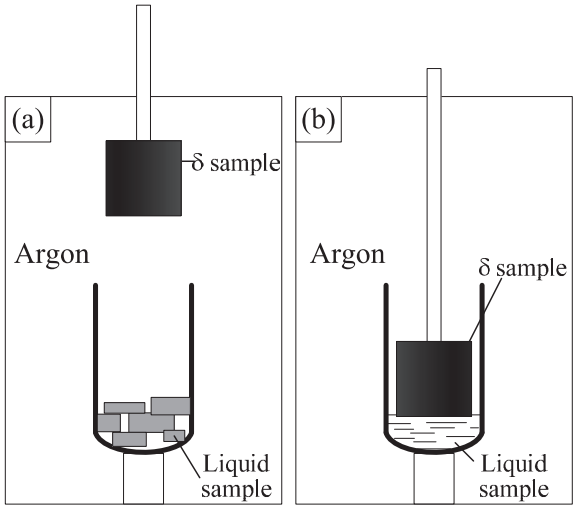

Fig. 2. Schematic drawing of the experimental procedures including (a) initial positions of the two samples and (b) contact of two samples.

3. Phase Field Simulation

In order to check the validity of the experimental findings, we performed phase field simulations. An accurate computation of peritectic reaction and transformation requires a quantitative phase-field model which should be constructed based on thin-interface limit. A quantitative multi-phase field model for the peritectic reaction and transformation has been recently developed by our group.[20] However, in present study, for some limitations and uncertain parameters which will be explained later, our focus is restricted to qualitative simulation. Hence, a multi-phase field model proposed by Steinbach and Pezzola[21,22] was utilized to see the particle effect qualitatively. A set of order parameters $\{\phi_i\}$ was introduced to distinguish different phases. Here, the subscript i of ϕ_i with i=L, γ, δ and p specifies liquid, γ, δ phases and the insolvable particle. ϕ_i is allowed to vary continuously from 0 to 1. ϕ_i satisfies the normalization condition, $\sum \phi_i = 1$, where the summation is carried out over all i. The concentration, c, is given by, $c = \sum_{i=1}^{n} \phi_i \, c_i$, with the concentration associated with i phase, c_i.

The time evolution of ϕ_i is described by the following equation,

$$\frac{\partial \phi_i}{\partial t} = -\frac{2}{N}\sum_{j \neq i}^{n} s_{ij} M_{ij} \left[\frac{\delta F}{\delta \phi_i} - \frac{\delta F}{\delta \phi_j} \right], \quad \text{..... (1)}$$

where F is the free energy functional of the system, M_{ij} is the mobility of i/j interface. N is the number of coexisting phases at a given spatial point. s_{ij} takes 1 when i and j phases coexist and it takes 0 otherwise. The functional derivative in Eq. (1) is written as,

$$\frac{\delta F}{\delta \phi_i} = \sum_{j \neq i}^{n} \left[\frac{\varepsilon_{ij}^2}{2} \nabla^2 \phi_j + \omega_{ij} \phi_j \right] + \left(f_i^c - c_i f_c \right), \quad \text{..... (2)}$$

where ε_{ij} and ω_{ij} are the gradient energy coefficient and a height of parabolic potential between i and j phases, respectively. f_i^c is the free energy density of i phase and f_c is the chemical potential. In the derivation of Eq. (2), we introduced the condition of the equal chemical potential between the coexisting phases.[23] In dilute alloy system, the following relation can be used,

$$(f_i^c - c_i f_c) - (f_j^c - c_j f_c) \approx -\frac{RT}{V_m}\left\{ (c_i - c_j) - (c_i^{e,j} - c_j^{e,i}) \right\}, \quad \text{... (3)}$$

where R is gas constant, T is the temperature and V_m is molar volume. $c_i^{e,j}$ represents the concentration of i phase in equilibrium with j phase.

The time evolution of concentration, c, is described by,

$$\frac{\partial c}{\partial t} = \nabla \cdot \sum_{i=1}^{n} D_i \phi_i \nabla c_i = \nabla \cdot \sum_{i=1}^{n} D_i \phi_i k_{i\gamma} \nabla c_\gamma \quad \text{, ... (4)}$$

where D_i is diffusion coefficient in i phase, $k_{i\gamma}$ is the partition coefficient defined as $k_{i\gamma}=c_i/c_\gamma$.

In Eq. (2), ε_{ij} and ω_{ij} are related to the interfacial energy between i and j phases, σ_{ij}, and the interface thickness, W, as follows,

$$\varepsilon_{ij} = \frac{2}{\pi}\sqrt{2W\sigma_{ij}} \quad \text{, ... (5)}$$

$$\omega_{ij} = \frac{4\sigma_{ij}}{W} \quad \text{..... (6)}$$

The mobility, M_{ij}, in Eq. (1) was assumed as follows,[8,20]

$$M_{ij} = \left(\frac{15}{4} \frac{a\varepsilon_{ij}^{\,2} RT_{m,ij}}{\omega_{ij} D_j} (1 - k_{ij})(c_i^{e,j} - c_j^{e,i}) \right)^{-1} \quad \text{, ... (7)}$$

where a=0.6276, and $T_{m,ij}$ is the transition temperature between i and j phases in pure iron.

We performed two-dimensional (2-D) simulations. The system is schematically shown in **Fig. 3**(a). The Neumann boundary condition was applied to x direction, while periodic boundary condition was applied to y direction. The total length of x axis was fixed at 300 μm, while the total length of y axis, l, was varied depending on fraction of particles. The initial thicknesses of the liquid and γ phases are about 50 and 1.5 μm, respectively. The temperature was set at 1 718 K. The insolvable particles are uniformly distributed in δ phase. We assumed carbon did not diffuse into the particles. Also, the particles that do not change the shape and position were considered by fixing the spatial profile ϕ_p during the whole transformation process. In order to fix ϕ_p, the interface mobility related to the particle, $M_{\gamma p}$ and $M_{\delta p}$, and carbon diffusion coefficient of the particle, D_p, are set to zero. Under this condition, ϕ_p was not changed with time, viz., $\partial\phi_p/\partial t$=0 and ϕ_γ, ϕ_δ change in time satisfying the normalization condition ($\phi_p+\phi_\delta+\phi_\gamma$=1). The initial concentrations of liquid and δ phases were set to $c_L^{e,\gamma}$ and $c_\delta^{e,\gamma}$, respectively. The initial concentration in γ phase was continuously changed from $c_\gamma^{e,L}$ at L/γ interface to $c_\gamma^{e,\delta}$ at

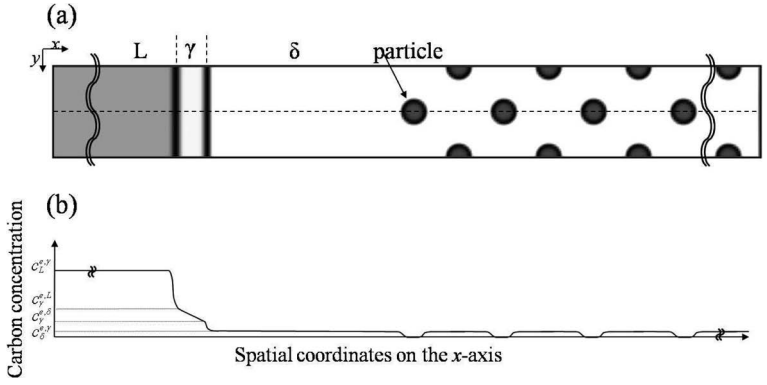

Fig. 3. (a) schematic drawing of phase field system and (b) initial carbon concentration profile along x-axis.

Table 1. Parameter values in simulation.

parameter	symbol	value [unit]
system size	–	$300\times l$ [μm^2] (l is inter-particle spacing)
mesh size	Δx	10^{-7} [m]
	Δy	10^{-7} [m]
time step	Δt	0.5×10^{-6} [s]
interface width	W	$7.0\times\Delta x$ [m]
molar volume[20]	V_m	7.7×10^{-6} [m^3 mol^{-1}]
interfacial energy[20]	$\sigma_{\delta/\gamma}$	0.370 [J m^{-2}]
	$\sigma_{L/\gamma}$	0.319 [J m^{-2}]
	$\sigma_{p/\gamma}$	0.370 [J m^{-2}]
	$\sigma_{p/\delta}$	0.370 [J m^{-2}]
diffusion coefficient[20]	D_γ	$7.61\times10^{-6}\exp(-13.7\times10^4/RT)$ [m^2 s^{-1}]
	D_δ	$1.27\times10^{-6}\exp(-8.3\times10^4/RT)$ [m^2 s^{-1}]
	D_L	$5.20\times10^{-6}\exp(-5.0\times10^4/RT)$ [m^2 s^{-1}]
	D_p	0 [m^2 s^{-1}]
$i\rightarrow j$ phase transition temperature of pure iron[20]	$T_{m,\gamma\delta}$	1 399 [K]
	$T_{m,\gamma L}$	1 801 [K]

δ/γ interface. The initial carbon concentration profile is shown in Fig. 3(b). The parameters used in the present simulations are summarized in **Table 1**.

It is noted that three-dimensional (3-D) simulations are essentially required for comparison with the experimental results. In terms of computational cost, however, our simulations are restricted to 2-D system. In the present discussion about simulations, for the sake of convenience, the total area of particles per unit area is called as volume fraction, f_v, instead of area fraction. In the simulations, the volume fraction, f_v was varied from 0.0 to 0.3. The particle radius, r was fixed at 0.5 μm. The interfacial energy between particle and δ phase, $\sigma_{p/\delta}$, and that between particle and γ phase, $\sigma_{p/\gamma}$, were assumed to be the same as $\sigma_{\delta/\gamma}$, because no exact value about the interfacial energy between ZrO_2 particles and matrix was reported.

As mentioned above, our simulations are limited to 2-D system and the system size and particle size are not comparable to the present experiment conditions. In addition, the present multi-phase field model essentially suffers from anomalous interface effects[20,24] which makes it quite difficult to perform quantitatively accurate simulations under a given set of input parameters. Importantly, a large uncertainty involves in the values of $\sigma_{p/\delta}$ and $\sigma_{p/\gamma}$ assumed in this study. In the light of these facts, the present simulations are not meant to be carried out to obtain accurate results which can be quantitatively compared with the experiment results. The present simulation was used to qualitatively check the validity of the experimental findings.

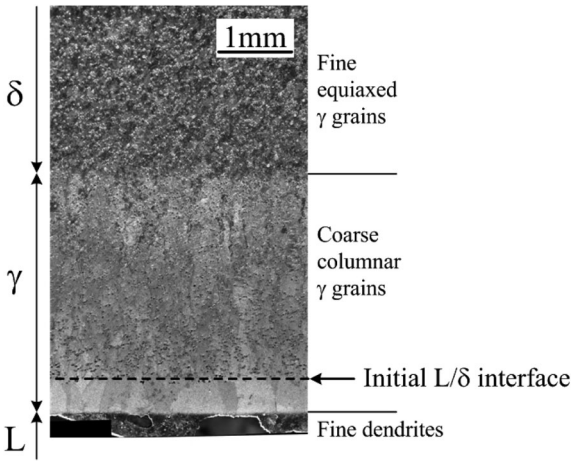

Fig. 4. Microstructure on the longitudinal section of sample having ZrO_2 particles of r=15 μm and f_v=0.1, quenched after holding at 1 718 K for 1 hour.

4. Results and Discussion

Figure 4 presents a longitudinal section of a sample having ZrO_2 particles with r=15 μm and f_v=0.1 and held at 1 718 K for 1 hour. Three different regions, viz., fine equiaxed γ grains, coarse columnar γ grains and very fine dendrites are observed from top to the bottom of this figure as indicated on the right-hand side in Fig. 4. These regions correspond to δ, γ and liquid phases before quenching as indicated on the left-hand side in Fig. 4. The positions of δ/γ and L/γ interfaces were apparently specified based on the difference in microstructure. Additionally, since ZrO_2 particles initially exist in only δ phase region, the initial L/δ interface can be clearly identified, which is marked as a dash line inside Fig. 4. The spherical ZrO_2 particles are randomly distributed in γ and δ phases above the initial interface. The upper and lower parts of the γ phase from the initial interface correspond to γ phase transformed from δ phase and that solidified from liquid phase, respectively. Therefore, the thickness of γ phase produced from δ phase and that from liquid phase can be separately measured.

Figure 5 shows the relationships between square root of holding time and the thickness of γ phase transformed from δ phase. In Fig. 5(a), the results for different volume fractions, f_v=0.02, 0.1 and 0.3 are shown. The radius of ZrO_2 particles is 50 μm in all the cases. The thickness of γ phase in each sample increases with the holding time. The result for f_v=0.1 is not obviously different from that for f_v=0.02. However, the thickness for f_v=0.3 is always smaller than those for f_v=0.02 and 0.1 at each period of time. Namely, the addition of ZrO_2 particles in δ phase retards the migration of δ/γ interface, indicating that there exists the retarding effect of particle on δ/γ interface. In Fig. 5(b), the results of different particle radii for f_v=0.1 are compared. One can see that the finer particle size results in the smaller thickness of γ phase. The retarding effect emerges even with f_v=0.1 when the particle size is small. These experimental results demonstrate that the insolvable particles in δ phase play a role of pin in migration of δ/γ interface. This retarding effect becomes stronger with a higher volume fraction and/or

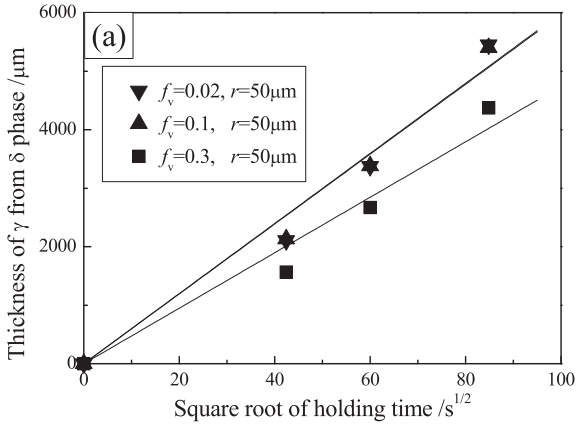

Fig. 5. Effects of (a) volume fraction, f_v, and (b) radius, r, of ZrO_2 particles on the growth of γ phase during δ to γ transformation at 1 718 K.

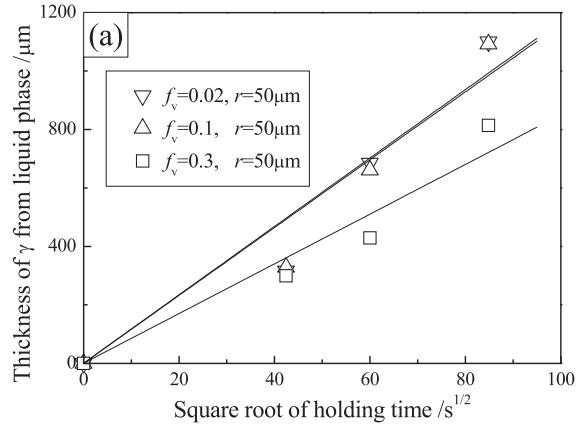

Fig. 6. Effects of (a) volume fraction, f_v, and (b) radius, r, of ZrO_2 particles on the growth of γ phase during liquid to γ solidification at 1 718 K.

smaller radius of insolvable particles. The fitting lines in Figs. 5(a) and 5(b) also clearly show this tendency, although the deviation with the plots exists due to the limited plots.

Figure 6 shows the relationships between square root of holding time and the thickness of γ phase solidified from liquid phase. It should be noted that L/γ interface does not directly interact with ZrO_2 particles. However, the migration of L/γ interface was clearly retarded by the addition of ZrO_2 particles. This retarding effect becomes significant when f_v is large and/or r is small, as is similar to the case of δ/γ interface.

In early diffusion couple experiments for δ/γ and L/γ interface motion,[9,10] it was shown that the growth of γ phase during peritectic transformation in Fe–C system is controlled by the carbon diffusion in γ phase from liquid to δ phases and the time dependence of thickness is described by the following parabolic rate law,

$$x = a_{i/j}\sqrt{t} \quad \text{..... (8)}$$

where x (μm) is the thickness of γ phase, t (s) is the holding time and $a_{i/j}$ (μm/s$^{1/2}$) is called parabolic constant for i/j interface. As shown in Figs. 5 and 6, the results with existence of ZrO_2 particles can be described by the parabolic rate law. The parabolic rate constants obtained in the present experiments are summarized in **Table 2**. A low value of $a_{i/j}$ indicates a low velocity of migration of i/j interface. Hence, the value of $a_{i/j}$ can be considered as a measure of how strong the retarding effect exists.

As mentioned above, when δ/γ interface is intersecting with the particles, it is bent, which causes the increase of total amount of interfacial energy and leads to the retardation of δ/γ interface migration. According to the Zener pinning theory, the pinning pressure P_Z on δ/γ interface migration due to all particles in unit area can be calculated as follows, [25]

$$P_Z = \frac{3f_v\sigma_{\delta/\gamma}}{2r} \quad \text{..... (9)}$$

This equation suggests that the dragging force increases with increase in f_v and decrease in r. Hence, our experimental results regarding δ/γ interface are qualitatively consistent with the Zener pinning theory. On the other hand, the retardation of L/γ interface observed in Fig. 6 and Table 2 will be discussed later.

The effect of second phase particle on peritectic transformation has been demonstrated by discussing the experimental facts. However, the behavior of moving δ/γ and L/γ interfaces during peritectic transformation is not clear from the microstructure of quenched sample shown in Fig. 4. More-

Table 2. Parabolic constant regressed from experimental data.

$r(\mu m)$, f_v of particle	50, 0.02	50, 0.1	50, 0.3	15, 0.1
$a_{\delta/\gamma}$(μm/s$^{1/2}$)	59.9	59.7	47.4	50.8
$a_{L/\gamma}$(μm/s$^{1/2}$)	11.7	11.6	8.5	7.8

$a_{\delta/\gamma}$: parabolic constant of δ/γ interface; $a_{L/\gamma}$: parabolic constant of L/γ interface.

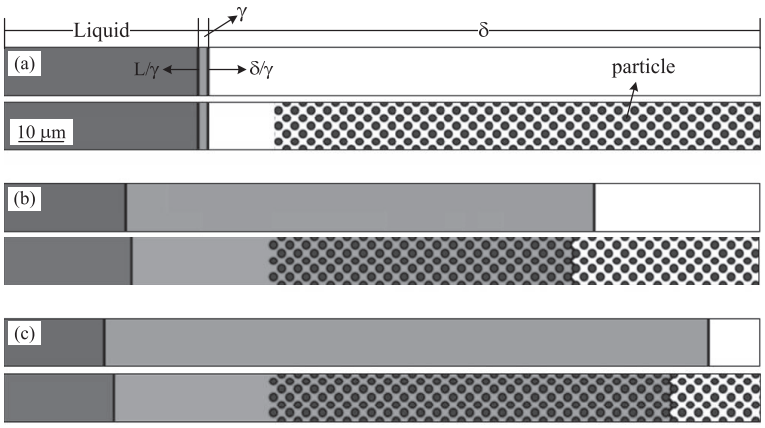

Fig. 7. Moving interface migration behavior in no particle case and particle case (f_v=0.3 and r=0.5 μm) at (a) t=0, (b) t=1.2 sec, (c) t=2.0 sec calculated by the multi-phase field simulation. Dark grey region, grey region, bright region and black circular region correspond to liquid, γ, δ phases and particles, respectively.

over, to check the validity of the experimental results, especially the effect of particle in δ phase on migration of L/γ interface, and to get better understanding of them, we performed 2-D phase field simulations. The simulated results are discussed as follows.

The time evolution of moving interfaces is shown in **Fig. 7**. One can see that γ phase grows toward δ and liquid phases. In Figs. 7(b) and 7(c), it's obvious that the velocity of both δ/γ and L/γ interfaces with the existence of particles is lower than that in no particle case. Importantly, when δ/γ interface is intersecting with the particles as shown in Fig. 7(b), it is bent by particle. The total amount of interfacial energy depends on the length of interface in case of 2-D. The bent process involves increasing length of δ/γ interface due to the change of its shape. Hence, the increment of total amount of interfacial energy occurs when the interface passes over the particle and therefore the migration of δ/γ interface should be retarded. The results of phase field simulations for time dependences of thickness of γ transformed from δ and liquid phases are shown in **Fig. 8**(a). These dependences are described well by the parabolic rate law given by Eq. (8). The calculated parabolic rate constants of δ/γ interface and L/γ interface are plotted in Fig. 8(b). Both $a_{\delta/\gamma}$and $a_{L/\gamma}$decrease with increase in volume fraction. More specifically, the existence of particle in δ phase retards the migration of δ/γ interface and it also reduces the migration velocity of L/γ interface. This retarding effect becomes strong as the volume fraction of particle increases. These are in good agreement with the experimental findings shown in Figs. 5(a) and 6(a) and Table 2.

As shown in Figs. 6 and 8, the migration of L/γ interface is retarded when the pinning particles exist in δ phase. This phenomenon is discussed. During peritectic transformation, the carbon diffuses in γ phase from liquid to δ phases. Because of the mass balance of carbon, the migration of L/γ interface is not irrelevant to the migration of δ/γ interface. When the migration of the δ/γ interface is slowed down due to the dispersion of particles in δ phase, the consumption of carbon by the δ to γ transformation decreases, which reduces carbon supply from the L to γ solidification. Thus, the migration of L/γ interface is also retarded by the dispersion of particles in δ phase.

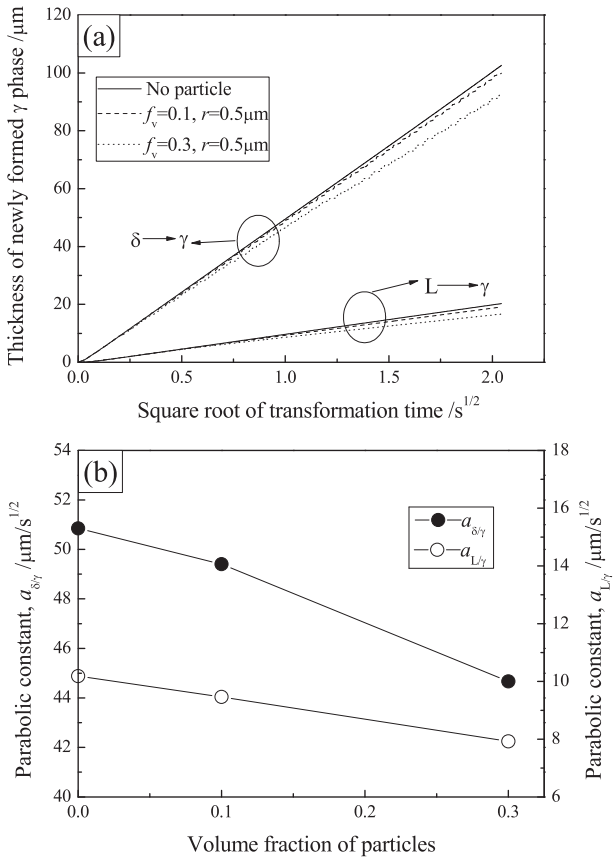

Fig. 8. Results of phase field simulations showing (a) time dependences of thickness of newly formed γ phase from δ and liquid phases (b) effects of particles on parabolic constant.

5. Conclusions

The effects of second phase particles on the peritectic transformation behavior in an Fe–C system was studied by performing a model experiment using diffusion couple method, in which the migration of δ/γ and L/γ interfaces was separately measured. The findings in the experimental work were verified by multi-phase field simulations. The results are summarized below.

(1) The migration of δ/γ interface is inhibited by the dispersion of second phase particles in δ phase. This inhibition

effect becomes significant by increasing f_v from 0.1 to 0.3 with r=50 μm or decreasing r=50 to 15 μm with f_v=0.1.

(2) Although the migration of L/γ interface does not meet any particle, it is also retarded by the presence of particles in δ phase. This is because of the mass balance of carbon during peritectic transformation. The retarding effect on δ/γ interface leads to an indirect effect of retardation on L/γ interface.

REFERENCES

1) Y. Maehara, K. Yasumoto, Y. Sugitani and K. Gunji: *Tetsu-to-Hagané*, **71** (1985), 1534.
2) M. Ohno and K. Matsuura: *ISIJ Int.*, **48** (2008), 1373.
3) S. Tsuchiya, M. Ohno, K. Matsuura and K. Isobe: *Tetsu-to-Hagané*, **95** (2009), 1.
4) S. Kencana, M. Ohno, K. Matsuura and K. Isobe: *ISIJ Int.*, **50** (2010), 231.
5) S. Kencana, M. Ohno, K. Matsuura and K. Isobe: *ISIJ Int.*, **50** (2010), 1965.
6) H. Shibata, Y. Arai, M. Suzuki and T. Emi: *Metall. Mater. Trans. B*, **31B** (2000), 981.
7) D. Phelan, M. Reid and R. Dippenaar: *Metall. Mater. Trans. A*, **7A** (2006), 985.
8) M. Ohno and K. Matsuura: *Acta Mater.*, **58** (2010), 6134.
9) K. Matsuura, Y. Itoh and T. Narita: *ISIJ Int.*, **33** (1993), 583.
10) K. Matsuura, H. Maruyama, Y. Itoh and K. Ishii: *ISIJ Int.*, **35** (1995), 183.
11) K. Matsuura, H. Maruyama, M. Kudoh and Y. Itoh: *ISIJ Int.*, **35** (1995), 1483.
12) K. Matsuura, M. Kudoh and T. Ohmi: *ISIJ Int.*, **35** (1995), 624.
13) K. Matsuura and M. Kudoh: *Mater. Trans., JIM*, **39** (1998), 203.
14) S. Morioka and H. Suito: *ISIJ Int.*, **48** (2008), 286.
15) A. V. Karasev and H. Suito: *ISIJ Int.*, **46** (2006), 718.
16) J. Janis, K. Nakajima, A. Karasev, H. Shibata and P. G. Jönsson: *J. Mater. Sci.*, **45** (2009), 2233.
17) M. Apel, B. Böttger, J. Rudnizki, P. Schaffnit and I. Steinbach: *ISIJ Int.*, **49** (2009), 1024.
18) C. S. Smith: *Trans. AIME*, **175** (1948).
19) T. B. Massalski: «Binary Alloy Phase Diagrams», Vol. 1, ASM, Materials Park, OH, (1986), 842.
20) M. Ohno and K. Matsuura: *Acta Mater.*, **58** (2010), 5749.
21) I. Steinbach and F. Pezzolla: *Physica D*, **134** (1999), 385.
22) J. Tiaden, B. Nestler, H. J. Diepers and I. Steinbach: *Physica D*, **115** (1998), 73.
23) S. G. Kim, W. T. Kim and T. Suzuki: *Phys. Rev. E*, **60** (1999), 7186.
24) R. F. Almgren: *SIAM J. Appl. Math.*, **59** (1999), 2086.
25) P. A. Manohar, M. Ferry and T. Chandra: *ISIJ Int.*, **38** (1998), 913.